Ionic fluids with r^{-6} pair interactions have power-law electrostatic screening

2005 J. Phys. A: Math. Gen. 38 5405

(http://iopscience.iop.org/0305-4470/38/24/002)

INSTITUTE OF PHYSICS PUBLISHING JOURNAL OF PHYSICS A: MATHEMATICAL AND GENERAL

J. Phys. A: Math. Gen. **38** (2005) 5405–5424 doi:10.1088/0305-4470/38/24/002

Ionic fluids with r^{-6} pair interactions have power-law electrostatic screening

Roland Kjellander and Björn Forsberg

Department of Chemistry, Physical Chemistry, Göteborg University, SE-412 96 Göteborg, Sweden

E-mail: rkj@chem.gu.se

Received 1 March 2005
Published 1 June 2005
Online at stacks.iop.org/JPhysA/38/5405

Abstract

The decay behaviour of radial distribution functions for large distances r is investigated for classical Coulomb fluids where the ions interact with an r^{-6} potential (e.g. a dispersion interaction) in addition to the Coulombic and the short-range repulsive potentials (e.g. a hard core). The pair distributions and the density–density (NN), charge–density (QN) and charge–charge (QQ) correlation functions are investigated analytically and by Monte Carlo simulations. It is found that the NN correlation function ultimately decays like r^{-6} for large r, just as it does for fluids of electroneutral particles interacting with an r^{-6} potential. The prefactor is proportional to the squared compressibility in both cases. The QN correlations decay in general like r^{-8} and the QQ correlations like r^{-10} in the ionic fluid. The average charge density around an ion decays generally like r^{-8} and the average electrostatic potential like r^{-6}. This behaviour is in stark contrast to the decay behaviour for classical Coulomb fluids in the absence of the r^{-6} potential, where all these functions decay exponentially for large r. The power-law decays are, however, the same as for quantum Coulomb fluids. This indicates that the inclusion of the dispersion interaction as an effective r^{-6} interaction potential in classical systems yields the same decay behaviour for the pair correlations as in quantum ionic systems. An exceptional case is the completely symmetric binary electrolyte for which only the NN correlation has a power-law decay but not the QQ correlations. These features are shown by an analysis of the bridge function.

PACS numbers: 05.20.Jj, 61.20.Gy, 61.20.Ja, 61.20.Qg

1. Introduction

For real Coulomb fluids such as plasmas, molten salts and electrolyte solutions, there is an ever-present r^{-6} van der Waals interaction between the particles. Still, in theoretical models

of such systems, one often does not include such interactions, e.g. in the classical Coulomb gas or in the primitive model of electrolyte solutions, where the ions are charged hard spheres and the solvent a dielectric continuum. In many cases, one may expect that the effect of the van der Waals interaction is just a rather weak perturbation on top of the electrostatic one, but this is not always true.

For colloidal dispersions, one has long recognized that both electrostatic and van der Waals interactions are very important, but in the standard theory for such systems, the Derjaguin–Landau–Verwey–Overbeek (DLVO) theory [1], one treats the two kinds of interactions as independent of each other and just adds them. It is of fundamental interest to see in what manner the two different kinds of interactions couple with each other. Also, for systems with highly polarizable ions, one can expect that interesting and important effects may arise that are described by power-law interactions. Even if the ions themselves do not have strong van der Waals interactions, they may have effective power-law interactions of a similar kind due to the surrounding solvent molecules. For instance, the absence of solvent molecules at the locations of the ions—i.e. voids in the solvent filled with individual ions—leads to an effective interaction between the voids of similar kind as between the solvent molecules.

For fluids of electroneutral particles interacting with an r^{-6} potential, it has been known for a long time that the pair distribution function has a tail that decays like r^{-6} with a prefactor proportional to the square of the compressibility. This result was conjectured by Enderby and coworkers [2]. Stell [3] later proved that it is formally correct. The same result is expected for ionic particles with an r^{-6} potential, which we indeed verify in this work. One implication of this is that on approach to a critical point where the compressibility approaches infinity, the r^{-6} tail becomes more important [4].

For the case of electroneutral particles, the behaviour of the pair distribution functions in the intermediate r range is dominated by oscillatory, exponentially decaying contributions [5]. The r^{-6} tails take over at long range. The presence of the r^{-6} potential precludes non-oscillatory exponential contributions, which are present in liquids with only finite-range interactions (e.g. hard sphere and square well potentials).

In models of ionic fluids in which there are no power-law interaction potentials in addition to the Coulomb potential, e.g. the classical Coulomb gas or the primitive-model electrolyte solutions, the pair distribution functions decay exponentially. The functional form of the decay is a Yukawa function $\exp(-\kappa r)/r$, where κ is a state-dependent decay constant, provided the density is sufficiently low. The same holds for the mean electrostatic potential from an ion in the ionic fluid, so the charges are exponentially screened (Debye screening). The common mean-field treatment of this kind of system is the Debye–Hückel (DH) approximation, where $\kappa = \kappa_D$ and κ_D^{-1} is the Debye length (see below for the definition of κ_D). The DH predictions are asymptotically exact in the limit of infinite dilution of the electrolyte. This is a rigorous result in classical statistical mechanics [6, 7].

It has been shown in analysis of the primitive model that the exponential Yukawa decay persists at higher concentrations, but now with $\kappa \neq \kappa_D$ [8–11]. In general, the density–density, charge–density and charge–charge correlations in the ionic fluid all decay exponentially with the same decay length κ^{-1} [12, 13]. A singular exception is the case of completely symmetric, binary electrolytes where the charge–density correlations are identically zero and the density–density and charge–charge correlations decay exponentially with different decay lengths (a completely symmetric electrolyte is one where the anions and cations differ only by the sign of their charges; often called the restricted primitive model (RPM)). The exponential decay length of the density–density correlations is $\geqslant(2\kappa)^{-1}$ for dilute systems in this case [11]).

In contrast to this, the exponential screening of charges does not hold true in quantum Coulomb fluids [6, 7]. The Debye screening is killed by the quantum fluctuations—essentially the same mechanism that causes the dispersion interaction. Instead one finds that the density–density correlations $h_{NN}(r)$ decay like r^{-6}, charge–density correlations $h_{QN}(r)$ like r^{-8} and the charge–charge correlations $h_{QQ}(r)$ like r^{-10}. The screening of charges is accordingly described by a power law and is not exponential. Thus, classical and quantum Coulomb fluids apparently behave in a fundamentally different manner in this respect.

A pertinent question is whether it is the lack of dispersion r^{-6} interactions in the model for classical Coulomb fluids that causes this discrepancy. This fundamental question is treated in the current work and the answer is yes. We find that provided an r^{-6} interaction is included as an effective pair potential, the decay behaviour of $h_{NN}(r)$, $h_{QN}(r)$ and $h_{QQ}(r)$ for large r values in the classical case is given by power laws with the same exponents as in the quantum case. This effective potential mimics the effects of the quantum fluctuations that are missing in the classical treatment.

An important aspect is what kind of electrostatic fluctuation interactions can be screened by electrolytes and which cannot because they occur on a much faster time scale than the rearrangement of ions. The dispersion force is of the latter type and therefore the r^{-6} tail survives in the intermolecular interaction and is not screened by fluctuations in ionic charge distributions. By adding the r^{-6} interaction term to the electrostatic pair potential in the classical treatment, one qualitatively includes effects of quantum fluctuations that are not screened.

A preliminary version of the current work has appeared in [14]. At the same time, Aqua and Fisher [4] published a study of ionic criticality with power-law forces in the special case of an exactly soluble spherical model of 1:1 lattice electrolytes. They found the same kind of power-law decay of the correlation functions in their simplified model as we did in the ionic fluid case.

Our approach is general and it shows that the r^{-6}, r^{-8} and r^{-10} decay behaviour of $h_{NN}(r)$, $h_{QN}(r)$ and $h_{QQ}(r)$, respectively, is an exact result in classical statistical mechanics for ionic fluids with r^{-6} potentials. This shows that the dispersion r^{-6} and Coulomb r^{-1} interactions couple in a non-trivial manner in classical fluids. Furthermore, it is shown in the current work that for a completely symmetric binary electrolyte (RPM electrolyte with added r^{-6} interaction, same for all species), it is only $h_{NN}(r)$ that decays like a power law. In this exceptional case $h_{QN}(r)$ and $h_{QQ}(r)$ do not have a power-law decay when the pair interactions have an r^{-6} contribution (h_{QN} is identically zero for symmetric electrolytes but h_{QQ} is not). Then the dispersion r^{-6} and Coulomb r^{-1} interactions are completely decoupled. This demonstrates that the completely symmetric electrolyte, which is commonly used to model electrolyte solutions, is a completely exceptional case and does not contain several phenomena, like this coupling. Thus it is in this respect an unsuitable model since it is too symmetrical. Any asymmetry will bring in the coupling.

Our results can be generalized to charged particles that interact with a non-Coulombic part of the pair potential decaying like $\gamma_{ij} r^{-\nu}$ with $\nu > 3$, where γ_{ij} is constant. Then $h_{NN}(r)$, $h_{QN}(r)$ and $h_{QQ}(r)$ decay in general like $r^{-\nu}$, $r^{-(\nu+2)}$ and $r^{-(\nu+4)}$ respectively. We shall, however, limit our explicit demonstration to the case $\nu = 6$.

The paper is organized as follows. In section 2, we first present the basic relationships on which our theoretical analysis is founded and we then proceed to the exact asymptotic analysis of the various correlation functions. In section 3, we present results from Monte Carlo simulations that confirm the theoretical analysis.

2. Theory

2.1. Basic definitions and relationships

We consider a binary ionic bulk fluid consisting of ions with charges q_i and number density n_i, where i is the species index. The ions interact with the pair potential

$$u_{ij}(r) = q_i q_j \phi(r) - \frac{\gamma_{ij}}{r^6} + u_{ij}^{\mathrm{sh}}(r), \tag{1}$$

where $\phi(r) = (4\pi\varepsilon_s\varepsilon_0 r)^{-1}$ is the Coulomb potential from a unit charge, ε_s is the dielectric constant of the solvent (if any), ε_0 is the permittivity of vacuum, γ_{ij} is a constant that gives the strength of the r^{-6} (e.g. dispersion) interaction between the ions, $r = |\mathbf{r}|$ and $\mathbf{r} = (x, y, z)$. The function $u_{ij}^{\mathrm{sh}}(r)$ contains the short-range repulsive interactions (for example the r^{-12} part of the Lennard-Jones potential or a hard core potential) and we will assume that it decays much faster to zero than r^{-6} when $r \to \infty$. This function may also include any other kind of short-range interaction.

We will use the notation $n = n_+ + n_-$ for the total ion concentration and $q = (n_+q_+ + n_-|q_-|)/n$ for a weighted average of the absolute value of the charge of the two species. It will also be useful to introduce the quantity $q_{\mathrm{Q}} = (q_+ + |q_-|)/2$. The Debye parameter κ_{D} and the associated Debye length κ_{D}^{-1} are defined from

$$\kappa_{\mathrm{D}}^2 = \frac{\beta}{\varepsilon_s\varepsilon_0}\sum_i n_i q_i^2 = \frac{\beta n q q_{\mathrm{Q}}}{\varepsilon_s\varepsilon_0}, \tag{2}$$

where $\beta = (k_{\mathrm{B}}T)^{-1}$, k_{B} is Boltzmann's constant and T the absolute temperature. The last equality follows from the relationship $nqq_{\mathrm{Q}} = n_+q_+^2 + n_-q_-^2$, where we have used the electroneutrality condition $n_+q_+ + n_-q_- = 0$.

The total correlation function $h_{ij}(r) = g_{ij}(r) - 1$, where $g_{ij}(r)$ is the radial distribution function, and the direct correlation function $c_{ij}(r)$ satisfies the Ornstein–Zernike (OZ) equation

$$h_{ij}(r) = c_{ij}(r) + \sum_l \int \mathrm{d}\mathbf{r}'\, c_{il}(|\mathbf{r} - \mathbf{r}'|) n_l h_{lj}(r'). \tag{3}$$

Furthermore, we have

$$c_{ij}(r) = -\beta u_{ij}(r) + h_{ij}(r) - \ln(1 + h_{ij}(r)) + e_{ij}(r), \tag{4}$$

where $e_{ij}(r)$ is the bridge function, which can be written as an infinite series of complicated integrals (bridge diagrams) that involve only the total correlation functions for all species and the ion density [15, 16]. Equation (4) implies

$$c_{ij}(r) + \beta u_{ij}(r) \sim \tfrac{1}{2}h_{ij}^2(r) + e_{ij}(r), \qquad \text{when} \quad r \to \infty. \tag{5}$$

For a fluid of uncharged particles interacting with a pair potential decaying like $-\gamma/r^\nu$, $\nu > 3$, it has been shown [3] that $h(r) \sim \beta K^2\gamma/r^\nu$ provided the system is not at a critical point. The constant K is dimensionless and proportional to the isothermal compressibility χ_T

$$K = k_{\mathrm{B}}Tn\chi_T = k_{\mathrm{B}}T\left(\frac{\partial n}{\partial P}\right)_{N,T}, \tag{6}$$

where N is the number of particles. In [3], it is shown that the right-hand side (rhs) of equation (5) decays like $C_1h^2(r)$, where C_1 is a constant, provided $h(r)$ decays like a power law with $\nu > 3$. Under these conditions we accordingly have $c(r) \sim \beta\gamma/r^\nu$ when $r \to \infty$. An important point, which we shall utilize below, is that a power-law decay in $h(r)$ with $\nu > 3$ accordingly only generates terms in $c(r)$ that decay much faster than the same power law.

For an ionic fluid in the absence of any power-law interactions apart from the Coulomb potential, we have $h_{ij}(r) \sim C_{ij}\exp(-\kappa r)/r$ when $r \to \infty$, at least for sufficiently low concentrations (the decay parameter $\kappa \neq \kappa_D$, but $\kappa/\kappa_D \to 1$ in the limit of infinite dilution). Provided that $h_{ij}(r)$ has this Yukawa-function decay, it has been shown [11] that the rhs of equation (5) decays proportional to $h_{ij}^2(r)/\ln^2 r$ or sometimes—for symmetric electrolytes or at higher concentrations—like $\exp(-\mu r)/r$ with $\mu \leqslant 2\kappa$. In the latter case the decay is slower than $h_{ij}^2(r)$, but it remains exponential. In any case the Coulomb interaction in ionic fluids generates by itself an exponential Yukawa decay or the product of an exponential function and a function that varies slower than any exponential (including sinusoidal functions, for instance when $h_{ij}(r)$ becomes oscillatory).

Thus, in our case we can use the usual asymptotic relationship for the direct correlation function $c_{ij}(r) \sim -\beta u_{ij}(r)$ when $r \to \infty$, but in an extended form that includes the two leading terms of equation (1) $c_{ij}(r) \sim -\beta q_i q_j \phi(r) + \beta\gamma_{ij}/r^6$. We will verify *a posteriori* that no power law with exponent smaller than 6 enters into $c_{ij}(r)$ (the highest exponent in $h_{ij}(r)$ turns out to be 6, so the corresponding contribution to $c_{ij}(r)$ will have exponent 12).

It is very useful to treat the Coulombic part of $c_{ij}(r)$ separately, so we define the remainder, $c_{ij}^0(r)$, from

$$c_{ij}(r) = c_{ij}^0(r) - \beta q_i q_j \phi(r). \tag{7}$$

It follows that this function decays like

$$c_{ij}^0(r) \sim \beta\gamma_{ij}/r^6, \qquad \text{when} \quad r \to \infty. \tag{8}$$

In this work we shall in particular be interested in the ionic density–density, charge–charge and charge–density distribution functions $h_{NN}(r)$, $h_{QQ}(r)$ and $h_{NQ}(r)$. For a general binary electrolyte they are related to $h_{ij}(r)$ by

$$\begin{aligned} h_{NN} &= \theta_+^2 h_{++} + 2\theta_+\theta_- h_{+-} + \theta_-^2 h_{--} \\ h_{QQ} &= \tfrac{1}{4}[h_{++} - 2h_{+-} + h_{--}] \\ h_{NQ} &= h_{QN} = \tfrac{1}{2}[\theta_+ h_{++} + (\theta_- - \theta_+)h_{+-} - \theta_- h_{--}], \end{aligned} \tag{9}$$

where $\theta_i = n_i/n$ is the fraction of i ions. Conversely, we have

$$h_{ij} = h_{NN} + (t_i + t_j)h_{NQ} + t_i t_j h_{QQ}, \tag{10}$$

where $t_l = q_l/q_Q$. We shall throughout this work use the notation that lowercase indices such as i and j will denote species, while uppercase indices such as I and J will denote N or Q. Equations (9) and (10) apply to all quantities with N and Q indices, not only correlation functions (see for example [13] for general relationships involving the N and Q indices used in this paper).

We introduce the functions $c_{IJ}(r)$ in analogy with the definition of $h_{IJ}(r)$ in equations (9). They satisfy the OZ equation

$$h_{IJ}(r) = c_{IJ}(r) + \sum_{L=N,Q} \int \mathrm{d}\mathbf{r}'\, c_{IL}(|\mathbf{r} - \mathbf{r}'|) n_L h_{LJ}(r') \tag{11}$$

provided we define n_L for $L = N, Q$ as follows [13]:

$$n_N = n \qquad n_Q = nq/q_Q. \tag{12}$$

In Fourier space the OZ equation (11) becomes

$$\hat{h}_{IJ}(k) = \hat{c}_{IJ}(k) + \sum_L \hat{c}_{IL}(k) n_L \hat{h}_{LJ}(k), \tag{13}$$

where we have used the following convention for the Fourier transform:

$$\hat{f}(k) = \int \mathrm{d}\mathbf{r}\, f(r)\, \mathrm{e}^{-\mathrm{i}\mathbf{k}\cdot\mathbf{r}} = \frac{4\pi}{k}\int_0^\infty \mathrm{d}r\, f(r) r \sin(kr). \tag{14}$$

In matrix form the OZ equation (13) can be written as $\hat{\mathbf{H}} = \hat{\mathbf{C}} + \hat{\mathbf{H}}\mathbf{N}\hat{\mathbf{C}}$, where we have defined the 2×2 matrices $\hat{\mathbf{H}} = \{\hat{h}_{IJ}(k)\}$, $\hat{\mathbf{C}} = \{\hat{c}_{IJ}(k)\}$ and $\mathbf{N} = \{n_I \delta_{IJ}\}$ and where δ_{IJ} is the Kronecker delta. The OZ equation can be written as

$$(\mathbf{1} + \hat{\mathbf{H}}\mathbf{N})(\mathbf{1} - \hat{\mathbf{C}}\mathbf{N}) = \mathbf{1}, \tag{15}$$

where $\mathbf{1}$ is the unit matrix.

For a sufficiently well behaved function $f(r)$ that decays to zero sufficiently rapidly when r increases, one can expand its Fourier transform $\hat{f}(k)$ in a Taylor series in k, which has only even powers of k. (This can be shown by inserting the Taylor series of $\sin(kr)$ in equation (14) and integrating termwise.) Functions that decay like a power law, e.g. our pair potential $u_{ij}(r)$ in equation (1), do not, however, belong to this group of functions. The Fourier transform of the Coulomb potential equals $\hat{\phi}(k) = (\varepsilon_s \varepsilon_0 k^2)^{-1}$ and the transform of a function that equals r^{-6} for $r \geqslant r_0$ but is finite for $0 \leqslant r < r_0$, where r_0 is an arbitrary positive number, contains a term $\pi^2|k|^3/12$ apart from terms with even powers of k. Since the anti-Fourier transform of $\pi^2|k|^3 \exp(-\tau|k|)/12$ goes to r^{-6} when $\tau \to 0$ for all r outside an infinitesimal neighbourhood of $r = 0$, one may say in a generalized way that $\pi^2|k|^3/12$ for practical purposes 'is' the Fourier transform of r^{-6} for $r > 0$. The behaviour of the function at the origin in r space is of no concern in our case since we are dealing with functions that are dominated by other contributions there (e.g. a hard core potential). In general,

$$f(r) \sim \frac{1}{r^{2(m+1)}} \qquad \text{when} \quad r \to \infty \quad \Leftrightarrow \quad \hat{f}(k) \text{ has } (-1)^m \frac{2\pi^2}{(2m)!} k^{2m-1} \tag{16}$$

as the term with lowest non-even power of k in the small k expansion of $\hat{f}(k)$ for $k > 0$.

From equations (7) and (9) applied to c_{ij} and c_{ij}^0, we obtain after some algebra

$$\hat{c}_{IJ}(k) = \begin{cases} \hat{c}^0_{QQ}(k) - \dfrac{\beta q_Q^2}{\varepsilon_s \varepsilon_0 k^2}, & \text{when} \quad I = J = Q \\ \hat{c}^0_{IJ}(k), & \text{otherwise.} \end{cases} \tag{17}$$

Furthermore, from equation (8) and the facts presented above we can conclude that

$$\hat{c}^0_{IJ}(k) = \hat{c}^0_{IJ}(0) + \hat{B}_{IJ}(k), \tag{18}$$

where for small k

$$\hat{B}_{IJ}(k) = \zeta^{(2)}_{IJ} k^2 + \frac{\pi^2 \beta \gamma_{IJ}}{12} k^3 + \zeta^{(4)}_{IJ} k^4 + O(k^6). \tag{19}$$

Here $\zeta^{(m)}_{IJ}$ are constants and γ_{IJ} is defined from γ_{ij} in analogy to equation (9). In equation (19) we have assumed that $u^{\mathrm{sh}}_{ij}(r)$ decays to zero at least as fast as r^{-10}. We have also utilized that the rhs of equation (5) gives a contribution that decays as fast as h^2, which will lead to a k^9 term as will be shown *a posteriori*. (These assumptions are stronger than what is actually needed.)

2.2. Asymptotic analysis

To determine the asymptotic behaviour of $h_{IJ}(r)$ when $r \to \infty$, we investigate the small k expansion of $\hat{h}_{IJ}(k)$. The behaviour of $h_{ij}(r)$ can then be found by using equation (10).

The expansion can be obtained from equations (15), (17)–(19) as demonstrated in appendix A. The result is

$$\begin{aligned}
\hat{h}_{NN}(k) &= \frac{K-1}{n} + \xi_{NN}^{(2)}k^2 + \frac{\pi^2\Lambda_{NN}}{12}k^3 + O(k^4),\\
\hat{h}_{NQ}(k) &= \sum_{m=1}^{2}\xi_{NQ}^{(2m)}k^{2m} + \frac{\pi^2\Lambda_{NQ}}{12}k^5 + O(k^6),\\
\hat{h}_{QQ}(k) &= \frac{1}{n_Q}\left(\frac{k^2}{\kappa_{\mathrm{D}}^2}-1\right) + \sum_{m=2}^{3}\xi_{QQ}^{(2m)}k^{2m} + \frac{\pi^2\Lambda_{QQ}}{12}k^7 + O(k^8),
\end{aligned} \tag{20}$$

where $\xi_{IJ}^{(2m)}$ are constants,

$$\begin{aligned}
&\Lambda_{NN} = \beta K^2\gamma_{NN}, \qquad \Lambda_{NQ} = \frac{\beta K}{\kappa_{\mathrm{D}}^2}[\gamma_{NQ} + K\tau n\gamma_{NN}],\\
&\Lambda_{QQ} = \frac{\beta}{\kappa_{\mathrm{D}}^4}[\gamma_{QQ} + 2K\tau n\gamma_{NQ} + (K\tau n)^2\gamma_{NN}]
\end{aligned} \tag{21}$$

and

$$\tau = \hat{c}_{NQ}^0(0) = \frac{1}{n^2 q}\sum_{ij} n_i n_j q_j \hat{c}_{ij}^0(0). \tag{22}$$

From equation (16) it therefore follows that

$$h_{NN}(r) \sim \frac{\Lambda_{NN}}{r^6}, \qquad h_{NQ}(r) \sim -30\frac{\Lambda_{NQ}}{r^8}$$

and

$$h_{QQ}(r) \sim 1680\frac{\Lambda_{QQ}}{r^{10}} \tag{23}$$

when $r \to \infty$. The numerical factors in the latter two equations are $(2m)!/4!$ for $m = 3$ and $m = 4$. The coefficient Λ_{NN} in the r^{-6} decay of $h_{NN}(r)$ is proportional to the square of the compressibility. It is the same as for a fluid of electroneutral particles with r^{-6} interactions.

Let us consider the special case when the coefficients for the r^{-6} potential in $u_{ij}(r)$ satisfy the common relationship $\gamma_{ij} = (\gamma_{ii}\gamma_{jj})^{1/2}$ ('mixing rule'), i.e. we can write

$$\beta\gamma_{ij} = \alpha_i\alpha_j, \tag{24}$$

where $\alpha_l = (\beta\gamma_{ll})^{1/2}$ for $l = i, j$. In this case we can simplify equation (21) since $\beta\gamma_{IJ} = \alpha_I\alpha_J$, where we have defined $\alpha_N = \theta_+\alpha_+ + \theta_-\alpha_-$ and $\alpha_Q = (\alpha_+ - \alpha_-)/2$. Then Λ_{QQ} in equation (21) can be written as a perfect square and Λ_{IJ} factorizes. We obtain

$$\Lambda_{IJ} = \lambda_I\lambda_J, \tag{25}$$

where

$$\lambda_N = K\alpha_N \tag{26}$$

and

$$\lambda_Q = \frac{1}{\kappa_{\mathrm{D}}^2}[\alpha_Q + K\tau n\alpha_N] = \frac{1}{\kappa_{\mathrm{D}}^2}\left[\alpha_Q + n\hat{c}_{NQ}^0(0)\lambda_N\right]. \tag{27}$$

Equation (25) implies the mixing rule

$$\Lambda_{QQ}\Lambda_{NN} = (\Lambda_{NQ})^2. \tag{28}$$

In the general case, the leading term in the decay of the ionic pair correlation function can be determined from equations (10) and (23). We have

$$h_{ij}(r) \sim \frac{\Lambda_{NN}}{r^6} \qquad \text{when} \quad r \to \infty, \tag{29}$$

i.e. the same for all species. The charge density around an ion of species i is given by

$$\rho_i(r) = \sum_j q_j n_j h_{ij}(r) = nq\left(h_{NQ}(r) + \frac{q_i}{q_Q} h_{QQ}(r)\right). \tag{30}$$

From equation (23) it follows that it decays like

$$\rho_i(r) \sim -30\frac{nq\Lambda_{NQ}}{r^8} \qquad \text{when} \quad r \to \infty.$$

Note that the sign of the tail is the same for anions and cations. The local electroneutrality condition

$$\int \rho_i(r)\,\mathrm{d}\mathbf{r} = \hat{\rho}_i(0) = nq\left(\hat{h}_{NQ}(0) + \frac{q_i}{q_Q}\hat{h}_{QQ}(0)\right) = -q_i \tag{31}$$

is, of course, fulfilled as it must be, which follows from equation (20) evaluated at $k = 0$. Likewise, the second moment condition is fulfilled, which follows from the k^2 term of $\hat{h}_{QQ}(k)$ in equation (20).

The electrostatic potential $\psi_i(r)$ at distance r from an ion of species i satisfies Poisson's equation

$$-\varepsilon_s\varepsilon_0\nabla^2\psi_i(r) = \rho_i(r) \tag{32}$$

for $r > 0$ and decays like

$$\psi_i(r) \sim \frac{nq\Lambda_{NQ}}{\varepsilon_s\varepsilon_0 r^6} \qquad \text{when} \quad r \to \infty. \tag{33}$$

Thus the presence of the r^{-6} potential in $u_{ij}(r)$ of the electrolyte has made the decay of the electrostatic potential follow an r^{-6} power law instead of the exponential decay it has in the absence of any power-law pair potential (i.e. apart from the Coulomb potential). Thus, the exponential screening in the electrolyte is ultimately replaced by a power-law screening for large r.

The leading power-law decay of charge density $\rho_i(r)$ and potential $\psi_i(r)$ is somewhat different for a symmetric binary electrolyte with $\gamma_{++} = \gamma_{--}$, for which $h_{++}(r) = h_{--}(r)$. Then $h_{NQ}(r)$ is identically zero, $q = q_Q = |q_i|$, $n = n_Q$ and $\rho_i(r) = q_i n h_{QQ}(r)$. Thus

$$\rho_\pm(r) \sim \pm 1680\frac{nq\Lambda_{QQ}}{r^{10}} \qquad \text{when} \quad r \to \infty \tag{34}$$

and

$$\psi_\pm(r) \sim \mp 30\frac{nq\Lambda_{QQ}}{\varepsilon_s\varepsilon_0 r^8} \qquad \text{when} \quad r \to \infty. \tag{35}$$

Note that the sign of $\rho_i(r)$ for large r is *equal* to that of the charge of the central ion if $\Lambda_{QQ} > 0$.

Finally, we shall treat the special case of a *completely* symmetric electrolyte for which the $-\gamma/r^6$ pair potential is the same for all species, $\gamma_{ij} = \gamma$ (e.g. restricted primitive model with an added $-\gamma/r^6$ potential). In this case the mixing rule $\gamma_{ij} = (\gamma_{ii}\gamma_{jj})^{1/2}$ is satisfied. Then $\Lambda_{QQ} = 0$ and the above results are irrelevant since the leading term we found vanishes. The detailed analysis of this case is presented in appendix B and is based on an investigation of a cluster expansion of the bridge function $e_{ij}(r)$ in equation (4). The results are quite

dramatic since we find that there is *no power-law term* in $h_{QQ}(r)$! Thus $h_{QQ}(r)$ does not have a power-law decay in this case ($h_{NQ}(r)$ is zero as before). Thus, the charge density $\rho_i(r)$ and potential $\psi_i(r)$ decay faster than any power law. On the other hand, $h_{NN}(r)$ decays as Λ_{NN}/r^6 like in equation (23). Therefore $h_{ij}(r)$ decays as in equation (29), which follows from equation (10). In the completely symmetric electrolyte, the r^{-6} and the Coulomb interactions are accordingly decoupled. This decoupling is destroyed by any asymmetry between anions and cations.

3. Simulation studies of the decay

To confirm the theoretical predictions for the decay of $h_{IJ}(r)$ in equation (23), we have performed Monte Carlo simulations of an ionic fluid with the following pair interaction potential:

$$u_{ij}(r) = u_{ij}^{\mathrm{Coul}}(r) + u_{ij}^{(6)}(r) + u_{ij}^{\mathrm{core}}(r), \tag{36}$$

where

$$u_{ij}^{\mathrm{Coul}}(r) = q_i q_j \phi(r),$$

$$u_{ij}^{(6)}(r) = \begin{cases} -\dfrac{\gamma_{ij}}{r^6}, & r \geqslant \sigma \\ -\dfrac{\gamma_{ij}}{\sigma^6}, & r < \sigma \end{cases}$$

and

$$u_{ij}^{\mathrm{core}}(r) = \begin{cases} 0, & r \geqslant d \\ \infty, & r < d. \end{cases}$$

This constitutes the following choice of $u_{ij}^{\mathrm{sh}}(r)$ in equation (1)

$$u_{ij}^{\mathrm{sh}}(r) = \begin{cases} 0, & r \geqslant \sigma \\ \gamma_{ij}\left[\dfrac{1}{r^6} - \dfrac{1}{\sigma^6}\right], & d \leqslant r < \sigma \\ \infty, & r < d, \end{cases} \tag{37}$$

where the role of the r^{-6} bit is to remove the corresponding contribution in equation (1) for $r < \sigma$. The selection of $u_{ij}^{(6)}(r)$ with a suitable value of σ ensures that there is no strong attraction for small r values from this potential.

For systems like electrolyte solutions in water at room temperature, the effects of an r^{-6} term with realistic values of γ_{ij} in the ion–ion interactions are very small in the tail region. The r^{-6} asymptotic range for $h_{IJ}(r)$ then lies at such large r values that $h_{IJ}(r)$ has decayed to very small values. This makes it very difficult to investigate the tails with computer simulations with any reasonable accuracy. Our main objective in this work is, however, to test the theoretical predictions about the tails, so we have the freedom to select system parameters to make this feasible. Thus, we can select the parameters such that they do not necessarily represent a physically realizable system. This does *not* mean that these effects would always be small in all real systems of interest; we have just not focused on the task of finding suitable realistic cases in this work. For example, since the power-law tails in equation (23) all have the compressibility in the prefactor, one would expect the tails to be more prominent on approach to a critical point where $K \to \infty$. Other cases where one may expect important contributions of such tails are in colloidal systems where van der Waals interactions play a very important

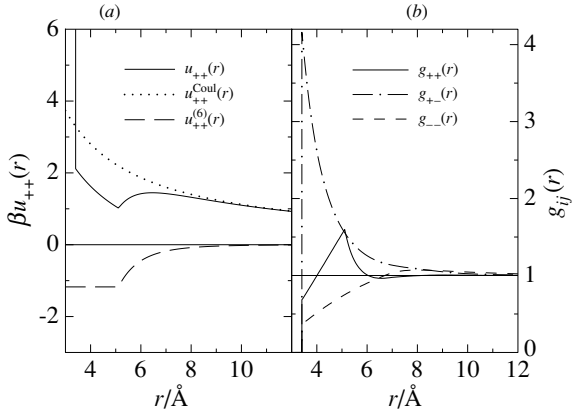

Figure 1. (*a*) The pair potential $u_{++}(r)$ in equation (36) used in the Monte Carlo simulations. The Coulomb term, $u_{++}^{\mathrm{Coul}}(r)$, and the r^{-6} term, $u_{++}^{(6)}(r)$, are also shown. The $--$ and $+-$ interactions (not shown) do not have the r^{-6} term since the coefficient γ_{ij} is zero in these cases. (*b*) The pair distribution functions $g_{ij}(r)$ from simulation II for an ionic fluid of monovalent ions with r^{-6} interaction at concentration 2 M (results for the same system are presented in all figures).

role. In the above derivation, we have not made any assumptions about the sizes and charges of the different species.

We have selected a system with sufficiently strong electrostatic coupling, so exponentially damped contributions to the ion–ion correlations decay away so rapidly that the power-law tails are exposed before they are very small and therefore difficult to calculate. The γ_{ij} values are selected as large as possible without causing aggregation of the particles. Still it requires a substantial simulation effort to reach sufficient precision. One needs a large number of particle configurations to achieve convergence of the small numerical values of pair correlation functions in the tails. Furthermore, because of the periodic boundary conditions one needs a large number of particles to represent these functions accurately for sufficiently large r values.

The simulated system consists of a 2 M 1:1 electrolyte with ionic hard core diameter $d =$ 3.4 Å. We have selected $\varepsilon_s T = 14\,907$ K, which corresponds to $\varepsilon_s = 50$ at room temperature. The r^{-6} parameters are $\beta\gamma_{++} = 2.09 \times 10^4$ Å^6, $\gamma_{+-} = \gamma_{--} = 0$ and $\sigma = 5.11$ Å. This choice of γ_{ij} satisfies equation (24) with $\alpha_- = 0$. Note that the electrolyte must be asymmetric (i.e. anions and cations must differ by something more than the sign of their charges) for Λ_{NQ} and Λ_{QQ} to be non-zero. The potential for the ++ interaction is shown in figure 1(*a*). The electrostatic part of the interaction potential was calculated using the minimal image convention, while a cut-off of half the simulation box length was used for the r^{-6} potential.

We have done three MC simulations in the canonical ensemble using the standard Metropolis algorithm [17]: *simulation I* with $N = 2000$ ions which was equilibrated for 1000 cycles and then sampled for 4 million cycles, *simulation II* with $N = 20\,000$ ions which was equilibrated for 4000 cycles and then sampled for 81 000 cycles and *simulation III* with $N = 30\,000$ ions which was equilibrated for 2000 cycles and then sampled during 18 300 cycles. (During one cycle all particles in the system are subject to one trial move each.) The cubic simulation box edges were 94.0, 202.5 and 231.8 Å respectively in the three cases.

The radial distribution functions $g_{ij}(r)$ were collected on a dense mesh. They are plotted for simulation II in figure 1(*b*). The peak for $g_{++}(r)$ is due to the local minimum of the $u_{++}(r)$ potential at the levelling-off radius of $u_{++}^{(6)}(r)$ at $r = 5.11$ Å. The functions $h_{IJ}(r)$ were

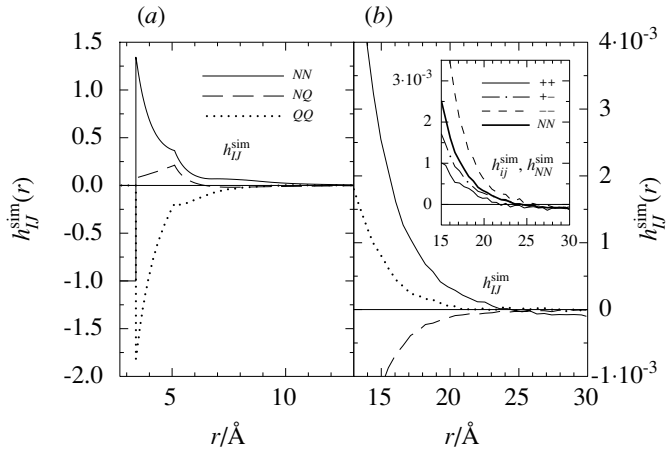

Figure 2. The density–density $h_{NN}(r)$, charge–density $h_{QN}(r) = h_{NQ}(r)$ and charge–charge $h_{QQ}(r)$ correlation functions from simulation II (superscript 'sim' indicates raw simulation data). (*a*) and (*b*) show these functions in different r ranges on different scales. The inset of (*b*) shows $h_{NN}(r)$ (thick curve) and $h_{ij}(r)$ (thin curves) for $i, j = +, -$.

calculated from equation (9) and they are shown in figure 2(*a*). The large r tail region of these functions is shown in figure 2(*b*) on a magnified scale. In this region, the data are given on a rather coarse mesh (spacing 0.54 Å) to reduce the noise in the data. The corresponding data from simulation I (not shown) contain less noise and that from simulation III (not shown) contain more noise because these simulations were run for larger/smaller number of cycles, respectively, compared to simulation II. We will use the notation $h_{ij}^{sim}(r)$ and $h_{IJ}^{sim}(r)$ with superscript 'sim' to indicate that we are dealing with the raw simulation data.

The inset of figure 2(*b*) shows the tail region of $h_{NN}^{sim}(r)$ and $h_{ij}^{sim}(r)$ for $i, j = +, -$. We see that these functions decay for large r to a negative number, h^{lim}, as they must for a system with a finite number of particles [18, 19]. This number is the same for $h_{NN}^{sim}(r)$ and $h_{ij}^{sim}(r)$. When the total number of particles, N, is increased to infinity and the density n is kept constant, h^{lim} tends asymptotically to zero as $-K/N$. The function $h_{NN}^{sim}(r)$ is plotted in figure 3(*a*) in the tail region for all three simulations (a magnified view of the simulation III curve is given in the inset). Clearly h^{lim} becomes less negative when N increases (going from simulations I to II to III).

On the other hand, for an infinite system the pair distribution functions $h_{ij}(r)$ approach zero for large r and so do $h_{IJ}(r)$. The latter functions satisfy

$$\int \mathbf{dr}\, h_{NN}(r) = (K - 1)/n \tag{38a}$$

$$\int \mathbf{dr}\, h_{NQ}(r) = 0 \tag{38b}$$

$$\int \mathbf{dr}\, h_{QQ}(r) = -1/n_Q, \tag{38c}$$

which follows from equation (20) at $k = 0$. Equation (38*a*) is equivalent to the fact that the density–density structure factor equals K at $k = 0$ (infinite wavelength). For a finite system (canonical ensemble) equations (38*b*) and (38*c*) are still satisfied, but instead of equation (38*a*)

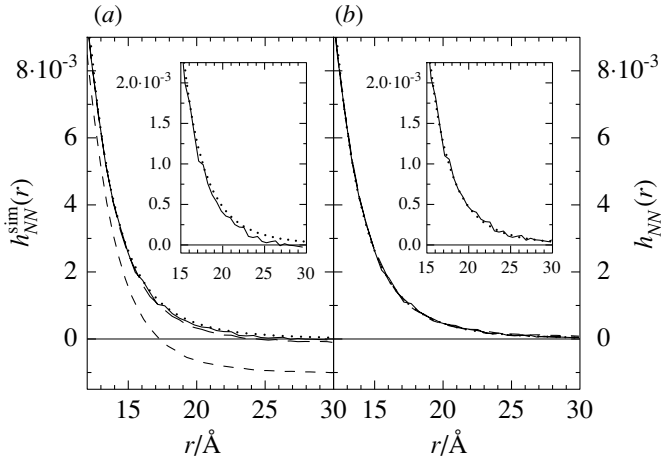

Figure 3. (*a*) The density–density correlation function before base line correction, $h_{NN}^{\rm sim}(r)$, from simulations I (short dashes), II (long dashes) and III (full line); superscript 'sim' indicates raw simulation data before correction. The curve from simulation II is the same as in figure 2. The dotted curve shows the function $3.0 \times 10^4/r^6$. The inset shows a magnified plot of the tail region for simulation III. (*b*) The functions $h_{NN}(r)$ for the same cases after base line correction. The dotted curve shows the function $3.0 \times 10^4/r^6$, same as in (*a*). The inset shows a magnified plot of the tail region for simulation III.

we have

$$\int_V \mathrm{d}\mathbf{r}\, h_{NN}(r) = -1/n, \tag{39}$$

where the integral is taken over the finite system volume V and $n = N/V$. The deviation of equation (39) from equation (38*a*) arises in the tail region where, as we have seen, $h_{NN}(r) \to h^{\rm lim} \approx -K/N$ for large r in the finite system.

Let us form a 'corrected' function by adding $|h^{\rm lim}|$ to $h_{NN}^{\rm sim}(r)$ inside V (except in the hard core region), i.e., we take

$$h_{NN}(r) = h_{NN}^{\rm sim}(r) - h^{\rm lim}. \tag{40}$$

The function $h_{NN}(r)$ thus obtained tends to zero for large r (inside V) and it satisfies equation (38*a*) to a good approximation (the approximation improves quickly when both N and V increase with N/V = constant). Thus, this function behaves approximately like $h_{NN}(r)$ for an infinite system. The latter function has practically decayed to zero outside V (provided V is sufficiently large), so we can take $h_{NN}(r) = 0$ outside V.

The functions $h_{NQ}(r)$ and $h_{QQ}(r)$ will not be affected as much by the finite system size effects. Their integrals always have the infinite system values, equations (38*b*) and (38*c*). The common limiting value $h^{\rm lim}$ of $h_{ij}(r)$ cancels in $h_{NQ}(r)$ and $h_{QQ}(r)$, see equation (9). Furthermore, these two functions can be written as linear combinations of $\rho_+(r)$ and $\rho_-(r)$ defined in equation (30) and $\rho_i(r)$ will approach zero at large r for electrostatic reasons. Thus we will take $h_{NQ}(r) = h_{NQ}^{\rm sim}(r)$ and $h_{QQ}(r) = h_{QQ}^{\rm sim}(r)$, i.e. as they come from the simulations without corrections.

We can calculate the value of $h^{\rm lim}$ from $h_{NN}^{\rm sim}(r)$ by requiring that equation (39) should be fulfilled when we set $h_{NN}^{\rm sim}(r) = h^{\rm lim}$ for $r > R$, where R is selected so large that the deviation of $h_{NN}^{\rm sim}(r)$ from $h^{\rm lim}$ gives a negligible contribution to the integral. Thereby contributions from the noise in the tail region of $h_{NN}^{\rm sim}(r)$ are eliminated. We have used this method to determine

$h^{\lim}$ for simulation III, which has the largest number of ions. In practice, a value of $R \geqslant 30$ Å is suitable for the present system. We set $h_{NN}^{\mathrm{sim}}(r) = h^{\lim}$ in the part of the simulation box outside radius $R = 30$ Å (this box is a cube with edges of length 231.8 Å) and use the simulation data for $r < R$. By selecting $h^{\lim}$ such that equation (39) is satisfied, we thus obtain $h^{\lim} = -6.7 \times 10^{-5}$.

When $|h^{\lim}| = 6.7 \times 10^{-5}$ is added to $h_{NN}^{\mathrm{sim}}(r)$ from simulation III (plotted in the inset of figure 3(*a*)), we obtain the full curve shown in the inset to figure 3(*b*). This curve practically coincides with the dotted curve, which is a graph of the function $3.0 \times 10^4/r^6$. Hence $h_{NN}(r)$ decays within the simulation error like the dotted curve. This holds in the interval 12–30 Å as shown in the main figure 3(*b*), i.e. within a value range of $h_{NN}(r)$ of about 2.5 orders of magnitude (from 10^{-2} down to 4×10^{-5}). Thus, the decay of $h_{NN}(r)$ is an inverse sixth power of r in agreement with the above analysis (at least in this interval).

From inspection of figure 3(*a*) we see that the deviation between the dotted curve and each of the curves from the three simulations is about constant in the range shown. Thus, the curves from all simulations can be made to practically coincide with the dotted one if they are shifted up by an appropriate amount. In figure 3(*b*) (the main frame), we see the results of adding 1.09×10^{-3} to the case I curve, 1.40×10^{-4} to case II and 6.7×10^{-5} (as before) to case III. Then, the three curves practically coincide with each other and, furthermore, they all decay as $3.0 \times 10^4/r^6$ in most of the range shown. (The shifts for simulations I and II were obtained by curve fitting to the dotted curve.) Hence, by using equation (23) we conclude that $\Lambda_{NN} = 3.0 \times 10^4$ Å^6 for this system. The $h_{NN}(r)$ simulation results used from now on in this paper are the corrected ones shown in figure 3(*b*).

To show even more convincingly that $h_{NN}(r)$ decays like Λ_{NN}/r^6 for large r, we have multiplied all $h_{IJ}(r)$ functions with r^6 and plotted the results in figure 4(*a*). Since r^6 is a pretty large number in the tail region, any inaccuracy will be blown up more and more for increasing r. We see that $r^6 h_{NN}(r)$ from simulation I is close to 3.0×10^4 between $r \approx 13$ and 22 Å, but starts to deviate systematically for $r > 22$ Å. This deviation can also be seen in figure 3(*b*) as a slight deviation of the dashed curve from the dotted for $r > 22$ Å. This tiny deviation becomes quite large when $h_{IJ}(r)$ is multiplied with r^6 and shows that the test in figure 4(*a*) is pretty stringent. The $r^6 h_{NN}(r)$ curves from simulations II and III are, however, constant within simulation error for $r > 13$ Å. The noise in the data is larger for the latter two simulations since they were run much fewer cycles than simulation I. The amplified noise due to the multiplication with r^6 has made us restrict the plot to a maximum r value of around 25 Å rather than 30 Å as in figure 3. The reason why $r^6 h_{NN}(r)$ from simulation I starts to deviate earlier than the other cases is probably that the simulation box is much smaller for I.

In figure 4(*a*), we also see that $r^6 h_{NQ}(r)$ and $r^6 h_{QQ}(r)$ do not tend to a constant. However, in figure 4(*b*) where we have multiplied all $h_{IJ}(r)$ functions with r^8, we see that $r^8 h_{NQ}(r)$ stays nearly constant for $r > 14$ Å in simulation III. The factor r^8 blows up the simulation noise quite a lot. One should consider that r^{-8} changes by about 2 orders of magnitude between 14 and 25 Å and that $h_{NQ}(r)$ is about 2×10^{-5} at $r = 25$ Å. Considering this small magnitude, the simulation results may be reliable only for $r < 23$ Å (indicated by a vertical line in the plot). In cases I and II there is a clear deviation for the largest r values. We see that in the interval $14 < r < 23$ Å the function has the constant value of -0.3×10^7 within the simulation error. From equation (23), we may thus conclude that $30\Lambda_{NQ} = 0.3 \times 10^7$ Å^8. The functions $r^8 h_{NN}(r)$ and $r^8 h_{QQ}(r)$ do not tend to a constant as expected.

In figure 4(*c*) we have multiplied all $h_{IJ}(r)$ functions with r^{10} and we see that $r^{10} h_{QQ}(r)$ stays nearly constant for $r > 15$ Å for case I, while it oscillates around the same value for cases II and III. One must remember that r^{-10} is a very rapidly decreasing function and has very small values in the range shown, so it is very tricky to calculate $h_{QQ}(r)$ accurately in a

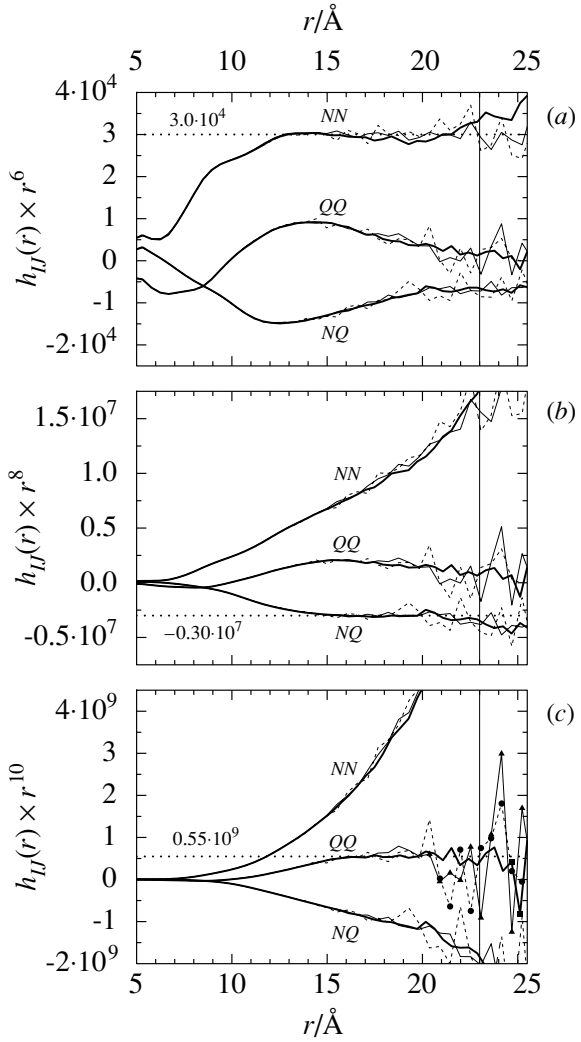

Figure 4. The functions $r^{\nu}h_{IJ}(r)$, $IJ = NN, NQ$ and QQ, plotted with different values of exponent: (*a*) $\nu = 6$, (*b*) $\nu = 8$ and (*c*) $\nu = 10$. The thick full curves show the results of simulation I, the thin full curves from simulation II and the dashed curves from simulation III. The horizontal dotted lines and the corresponding decimal numbers show the estimated levelling off value of the curves for $h_{NN}(r)$ in (*a*), $h_{NQ}(r)$ in (*b*) and $h_{QQ}(r)$ in (*c*). The symbols in (*c*) show the data points in the region where the simulation noise makes the data for $h_{QQ}(r)$ assuming both positive and negative values (simulation I, full squares; II, full triangles; III, full circles). The vertical line at $r = 23$ Å indicates that the amplified noise makes some of the curves $r^{\nu}h_{IJ}(r)$ less reliable to the right of the line.

simulation. The simulation errors are blown up a lot by the multiplication with r^{10}. The noise make the data points take on both positive and negative values for large r, while the correct $h_{QQ}(r)$ is small but positive. The data points where the simulated data oscillate on both sides of zero are indicated by symbols in figure 4(*c*). Despite these technical problems, it is quite reasonable to conclude that $h_{QQ}(r)$ decays like r^{-10} and we find that $1680\Lambda_{QQ} = 0.55 \times 10^9$ Å^{10}. Clearly, none of $r^{10}h_{NN}(r)$ and $r^{10}h_{NQ}(r)$ tend to a constant.

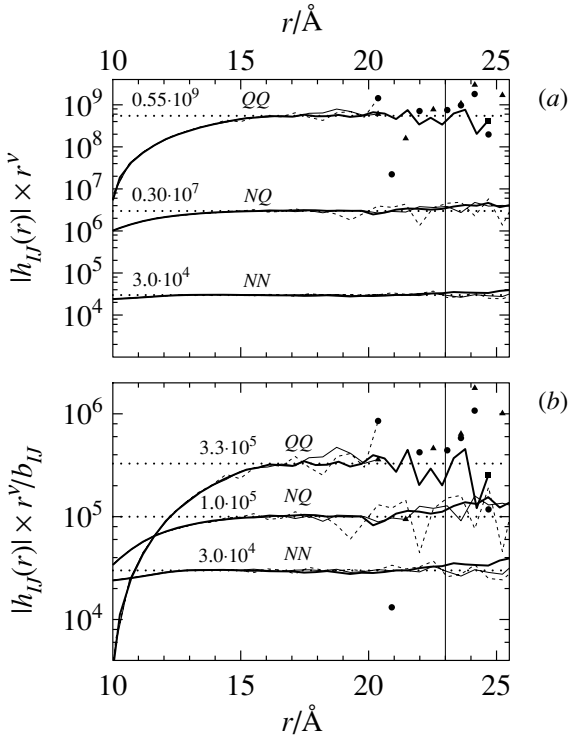

Figure 5. (*a*) The functions $r^{\nu}|h_{IJ}(r)|$ plotted on a logarithmic scale with different values of exponent: $\nu = 6$ for $IJ = NN$, $\nu = 8$ for NQ and $\nu = 10$ for QQ. Notation as in figure 4. The symbols show the positive data values for QQ in the region where the noise make the data assume both positive and negative values, which are unfit in a log plot even if we plot the absolute values. (*b*) The same plots but for the functions $r^{\nu}|h_{IJ}(r)|/b_{IJ}$, where $b_{NN} = 1$, $b_{NQ} = 30$ and $b_{QQ} = 1680$, see the text. The horizontal dotted lines and the corresponding decimal numbers show the estimated levelling off values of the curves in both (*a*) and (*b*).

The r interval where we see the levelling off in the plots is not so large, so one cannot rule out that some other functional form may fit the curves. Furthermore, the values of K calculated from $h^{\lim} \approx -K/N$ in the three simulations are somewhat different, where $h^{\lim}$ for simulations I and II are obtained from the shifts of $h_{NN}(r)$ needed to make the three simulations agree in figure 3(*b*). These K values do not quite agree with K calculated from Λ_{NN} using equation (21). These discrepancies are most likely due to finite simulation box size effects for the tails, which have very small values in the region we investigate and are therefore sensitive to the size. The asymptotic limiting forms we have derived are strictly true for infinite systems but not for finite ones.

There is, however, another quite independent test one can do about the correctness of the decay laws in equation (23). Since our choice of γ_{ij} satisfies equation (24), the coefficients Λ_{IJ} must obey the relationship (28). We obtained above $\Lambda_{NN} = 3.0 \times 10^4$ Å^6, $\Lambda_{NQ} = 1.0 \times 10^5$ Å^8 and $\Lambda_{QQ} = 3.3 \times 10^5$ Å^{10}. We have $\Lambda_{QQ}\Lambda_{NN} = 0.99 \times 10^{10}$ Å^{16} which should be compared with $(\Lambda_{NQ})^2 = 1.0 \times 10^{10}$ Å^{16}. Thus the levelling off values of the curves in figure 4 agree with what theory predicts.

Another way to see this is shown in figure 5. We have plotted $|h_{IJ}(r)|r^{\nu}$ on a logarithmic scale in figure 5(*a*) with $\nu = 6$ for NN, 8 for NQ and 10 for QQ. All curves level off at

the same value as before. Only the positive data points of $h_{QQ}(r)$ are plotted for large r (data points shown as symbols), where the simulation noise make some data points negative (cf figure 4(c)). In figure 5(b), we have divided the functions by the numerical factor $(2m)!/4!$ as predicted in equation (23), i.e. by $b_{NN} = 1$, $b_{NQ} = 30$ and $b_{QQ} = 1680$ respectively. We see that the flat parts of the curves now become equidistant on a log scale as required by equation (28). These findings give a very clear indication that the analysis about the limiting behaviour is correct. If the levelling off were fortuitous, it would be highly unlikely that the values would satisfy the theoretical requirement (28) of the prefactors.

Furthermore, the values $b_{IJ} = (2m)!/4!$ of the numerical factors in equation (23) are linked to the value of the exponent in the power-law decay. It would be unlikely that division by the values $b_{NN} = 1$, $b_{NQ} = 30$ and $b_{QQ} = 1680$ (associated with the power laws r^{-6}, r^{-8} and r^{-10}) would transform the nonequidistant curves in figure 5(a) to equidistant curves if the power-law decays that we found were incorrect.

To summarize, we have shown by simulation that the $h_{IJ}(r)$ functions decay as power laws in agreement with the theoretical analysis and furthermore that the relative magnitudes of the prefactors satisfy the theoretical predictions.

Acknowledgments

The authors are very grateful for discussions with George Stell. We thank him for making us aware of the quantum analogue of the power-law decays we found in the classical case. This work has received financial support from the Swedish Research Council.

Appendix A

In this appendix, we shall derive the small k expansion of $\hat{h}_{IJ}(k)$ shown in equation (20). From equations (15), (17) and (18) we obtain

$$\mathbf{1} + \hat{\mathbf{H}}\mathbf{N} = (\mathbf{1} - \hat{\mathbf{C}}\mathbf{N})^{-1} = \begin{pmatrix} A_{NN} - \hat{B}_{NN}n & A_{NQ} - \hat{B}_{NQ}n_Q \\ A_{QN} - \hat{B}_{QN}n & A_{QQ} - \hat{B}_{QQ}n_Q + \dfrac{\kappa_D^2}{k^2} \end{pmatrix}^{-1}, \tag{A.1}$$

where $\mathbf{A} = \mathbf{1} - \hat{\mathbf{C}}^0(0)\mathbf{N}$ is a constant matrix and we have used $n_Q q_Q^2 = nqq_Q$ and equation (2). By taking the inverse and multiplying and dividing all elements by k^2/κ_D^2, we obtain

$$\mathbf{1} + \hat{\mathbf{H}}\mathbf{N} = \frac{1}{A_{NN}(1-F)} \begin{pmatrix} 1 + \dfrac{k^2}{\kappa_D^2}(A_{QQ} - \hat{B}_{QQ}n_Q) & -\dfrac{k^2}{\kappa_D^2}(A_{NQ} - \hat{B}_{NQ}n_Q) \\ -\dfrac{k^2}{\kappa_D^2}(A_{QN} - \hat{B}_{QN}n) & \dfrac{k^2}{\kappa_D^2}(A_{NN} - \hat{B}_{NN}n) \end{pmatrix}, \tag{A.2}$$

where $1 - F = Dk^2/\left(A_{NN}\kappa_D^2\right)$ and D is the determinant of $\mathbf{1} - \hat{\mathbf{C}}\mathbf{N}$. We can write

$$F(k) = \frac{\hat{B}_{NN}n}{A_{NN}} - \frac{k^2}{\kappa_D^2}\left[(A_{QQ} - \hat{B}_{QQ}n_Q)\left(1 - \frac{\hat{B}_{NN}n}{A_{NN}}\right) - \frac{n}{n_Q A_{NN}}(A_{NQ} - \hat{B}_{NQ}n_Q)^2\right]. \tag{A.3}$$

The small k expansion of the rhs of equation (A.2) can now be obtained by expanding $1/(1 - F(k)) = 1 + F(k) + F^2(k) + O(k^6)$ in equation (A.2) and inserting equation (19).

By identifying the term with lowest odd-integer power in the k expansion of each element of the matrix, we can determine the corresponding contribution to $\hat{h}_{IJ}(k)$. After some algebra we find equation (20), where we have used

$$A_{NN} = 1 - n\hat{c}^0_{NN}(0) = 1 - \frac{1}{n}\sum_{ij} n_i n_j \hat{c}^0_{ij}(0) = \frac{\beta}{n\chi_T} = \frac{1}{K} \tag{A.4}$$

(cf [20]) and defined $\tau = -A_{NQ}/n_Q = \hat{c}^0_{NQ}(0)$, equation (22).

Appendix B

In this appendix, we shall treat completely symmetric binary electrolytes with a $-\gamma/r^6$ pair potential that is the same for all species (e.g. restricted primitive model with an added $-\gamma/r^6$ potential). Thus the anions and cations only differ by the sign of their charges. We shall show that only $h_{NN}(r)$ has a power-law decay, while $h_{QQ}(r)$ and $h_{NQ}(r)$ do not. For simplicity, we assume that the pair interaction potential has no other $r^{-\nu}$ potential with $\nu > 3$ apart from r^{-6} (this assumption is, however, not essential for the main results).

We shall initially make a less restrictive assumption. We only assume that the anion and cation charges are $q_+ = -q_- = q$, the ionic densities $n_+ = n_- = n/2$ and the non-electrostatic parts of the anion–anion and cation–cation pair interactions are identical. Thus the r^{-6} potential is given by $-\gamma_{ij}/r^6$ with $\gamma_{++} = \gamma_{--}$, but γ_{+-} may be different. We have $h_{++}(r) = h_{--}(r)$ and it follows from equation (9) that all quantities with index NQ are identically equal to zero, for instance $h_{NQ}(r) = 0$. As a consequence the Ornstein–Zernike equation for the NN and QQ functions decouples. The latter OZ equation can be written in Fourier space

$$1 + n\hat{h}_{QQ}(k) = \frac{1}{1 - n\hat{c}_{QQ}(k)} = \frac{1}{1 - n\hat{c}^0_{QQ}(k) + \kappa_D^2/k^2}, \tag{B.1}$$

where we have used that $q_Q = q$ and $n_Q = n$ for this case. By multiplying the numerator and the denominator by k^2/κ_D^2 and expanding the resulting function in a power series we obtain

$$1 + n\hat{h}_{QQ}(k) = \frac{k^2}{\kappa_D^2}\left[1 - \frac{k^2}{\kappa_D^2}\left(1 - n\hat{c}^0_{QQ}(k)\right) + \sum_{l=2}^{\infty} \frac{(-1)^l k^{2l}}{\kappa_D^{2l}}\left(1 - n\hat{c}^0_{QQ}(k)\right)^l\right]. \tag{B.2}$$

We now insert equations (18) and (19) for $IJ = QQ$ and identify the term with lowest odd-integer power of k. We see that this term originates from $k^4 n\hat{c}^0_{QQ}(k)/\kappa_D^4$ and equals $\pi^2\Lambda_{QQ}k^7/12$ with $\Lambda_{QQ} = \beta\gamma_{QQ}/\kappa_D^4$ in agreement with equations (20) and (21) when all quantities with index NQ are identically zero (including $\tau = \hat{c}^0_{NQ}(0)$). This gives rise to the leading r^{-10} term for $h_{QQ}(r)$ in equation (23).

For symmetric electrolytes $\gamma_{QQ} = (\gamma_{++} - \gamma_{+-})/2$, so we have $\gamma_{QQ} \neq 0$ only if $\gamma_{+-} \neq \gamma_{++} = \gamma_{--}$, which implies that the mixing rule $\gamma_{ij} = (\gamma_{ii}\gamma_{jj})^{1/2}$ is not satisfied. When

$$\gamma_{+-} = \gamma_{++} = \gamma_{--} = \gamma, \tag{B.3}$$

the mixing rule is satisfied and we have $\gamma_{QQ} = 0$ and $\gamma_{NN} = \gamma$. Hence no r^{-10} term appears in $h_{QQ}(r)$ in this case. On the other hand, the function $h_{NN}(r)$ decays as Λ_{NN}/r^6 with coefficient $\Lambda_{NN} = \beta K^2\gamma_{NN}$ as before.

To find the leading power-law term of the decay of $h_{QQ}(r)$ when $\gamma_{QQ} = 0$ we need to find the corresponding singular term in equation (B.2), which will still occur in $k^4 n\hat{c}^0_{QQ}(k)/\kappa_D^4$ (if it exists) since the other terms containing $\hat{c}^0_{QQ}$ are of higher order in k. Hence if $\hat{c}^0_{QQ}(r)$ decays like $r^{-\nu}$, the decay of $h_{QQ}(r)$ goes like $r^{-(\nu+4)}$ due to the factor k^4. Thus the decay behaviour of $h_{QQ}(r)$ follows from that of c^0_{QQ}. The asymptotic decay of the latter function can be inferred

from equations (4) and (7). We obtain (cf equation (5))

$$c^0_{QQ}(r) \sim \frac{\beta\gamma_{QQ}}{r^6} + h_{QQ}(r)h_{NN}(r) + e_{QQ}(r) \qquad \text{when} \quad r \to \infty, \tag{B.4}$$

where we have used that

$$h_{+\pm}(r) = h_{NN}(r) \pm h_{QQ}(r), \tag{B.5}$$

which follows from equation (10). Since $\gamma_{QQ} = 0$ the first term in the right hand side (rhs) of equation (B.4) is zero. The term $h_{QQ}(r)h_{NN}(r)$ decays like $h_{QQ}(r)\Lambda_{NN}/r^6$ and we shall now show that it cannot contain a leading power-law term of order $r^{-\nu}$ for $c^0_{QQ}(r)$, where ν is a positive integer. To demonstrate this, let us assume that $c^0_{QQ}(r)$ decays like $r^{-\nu}$. Then, as we have seen, $h_{QQ}(r)$ decays like $r^{-(\nu+4)}$. If $h_{QQ}(r)h_{NN}(r)$ contains the leading term of $c^0_{QQ}(r)$, it follows that the latter decays like $r^{-(\nu+10)}$, which is a contradiction to the assumption that $c^0_{QQ}(r)$ decays like $r^{-\nu}$ (a *reductio ad absurdum* argument). Thus $h_{QQ}(r)h_{NN}(r)$ cannot contain the leading $r^{-\nu}$ term (if it exists).

We shall now see that for very similar reasons, the bridge function $e_{QQ}(r)$ cannot contain any power-law term and as a consequence $c^0_{QQ}(r)$ and hence $h_{QQ}(r)$ *do not decay like a power law* when $\gamma_{QQ} = 0$ for a symmetric electrolyte.

We have $e_{QQ}(r) = (e_{++}(r) - e_{+-}(r))/2$. Let us expand the bridge function $e_{ij}(r_{12})$ in a cluster expansion with h bonds, density field points and two root points labelled 1 and 2 [15, 16]. Consider any diagram in the expansion. Replace each bond in the diagram with $h_{NN}(r) \pm h_{QQ}(r)$ according to equation (B.5). This diagram can then be written as a sum of diagrams, one with only h_{NN} bonds, several with various numbers of h_{NN} and h_{QQ} bonds and one with only h_{QQ} bonds. All resulting diagrams look the same except for the nature of the bonds. Let us do this operation for all diagrams in e_{ij}.

First we consider the diagrams in e_{ij} with only h_{NN} bonds. Since each ionic density field point (factor n_l) is summed over both species ($l = +$ and $-$) and since the bonds are independent of the species index, we can easily do the sums explicitly and instead obtain diagrams with *total density* field points (factor $n = n_+ + n_-$) and h_{NN} bonds. Let us compare the resulting diagrams in e_{++} and e_{+-}. The diagrams in e_{++} must be the same as those in e_{+-} since all bonds (including the bonds to the root points) are independent of species. For example, the following two diagrams must have the same value

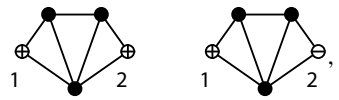

(B.6)

where the symbol in each open circle (root point) indicates the species index, the filled circles are field points and the lines are h_{NN} bonds. Hence, the diagrams of this kind in e_{++} cancel the corresponding diagrams in e_{+-} when we take the difference, so e_{QQ} will not contain any diagrams with only h_{NN} bonds.

Next we consider the diagrams in e_{ij} with one or more h_{QQ} bonds. We first treat the diagrams that contain at least one field point that is connected to the rest of the diagram with an odd number of h_{QQ} bonds, for example

(B.7)

where the thin lines are h_{NN} bonds and the thick lines are h_{QQ} bonds. Each h_{QQ} bond connected to a point is associated with a sign that depends on the species index, cf equation (B.5). Thus, when we do the species index sum at a field point ($l = +$ and $-$),

we obtain a factor $[(+1)^m + (-1)^m]n/2$, where m is the number of h_{QQ} bonds that connect to the point. When m is odd the factor is zero and hence the resulting diagram does not appear in e_{ij}.

On the other hand, for diagrams where all field points are connected to the rest of the diagram with even numbers (including zero) of h_{QQ} bonds, the species index sum results in a factor n for every field point, for example for the diagrams

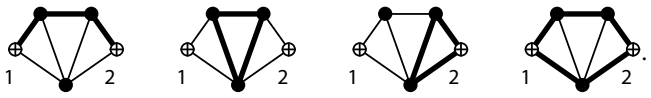

(B.8)

In this case, the resulting diagrams have total density (n) field points, h_{NN} and h_{QQ} bonds.

A bridge diagram does not have any nodes, and therefore, in each diagram there must exist at least two paths between points 1 and 2 that have no field points (and therefore no bonds) in common. Furthermore, since a bridge diagram does not have any articulation pair of points, each field point must have at least three bonds. Since each field point in e_{ij} must have an even number of h_{QQ} bonds (including zero), the h_{QQ} bonds form one or more continuous paths in each diagram—if there is an 'incoming' h_{QQ} bond to a field point there is also an 'outgoing' h_{QQ} bond in the path. Thereby, each h_{QQ} bond belongs to only one path. Furthermore, two paths are either disjoint or they are intersecting (or touching) each other at field points that have four or more h_{QQ} bonds.

Since the root points 1 and 2 can have an odd number of h_{QQ} bonds, it is possible for a path to 'begin' at one root point and 'finish' at the other (like in the leftmost diagram in (B.8)). Otherwise the paths must be closed loops. We shall first consider the latter category for which *all* points in each diagram (root and field points) have an even number of h_{QQ} bonds (including zero). Let us compare the diagrams of this kind in e_{++} and e_{+-}. The only difference is that the h_{QQ} bonds to root point 2 have different signs in e_{++} and e_{+-}. This makes each diagram in e_{+-} multiplied by $(-1)^{m_2}$, where m_2 is the number of h_{QQ} bonds of point 2. Otherwise the diagrams are identical to those in e_{++}. Since m_2 is even or zero, the diagrams in e_{++} and e_{+-} have the same values. For example, the following two diagrams must be equal

(B.9)

Thus these kinds of diagrams cancel in e_{QQ}. Note that the diagrams with only h_{NN} bonds, that we treated separately above, belong to this category.

The only remaining possibility is that both points 1 and 2 have odd numbers of h_{QQ} bonds, in which case at least one continuous path of h_{QQ} bonds connects the two root points. Then, the diagrams in e_{++} and e_{+-} have opposite signs (since m_2 is odd), for instance

(B.10)

The right diagram above must be minus the left diagram and therefore they *do not* cancel in e_{QQ}. From $e_{QQ}(r) = (e_{++}(r) - e_{+-}(r))/2$ it hence follows that e_{QQ} is equal to the sum of diagrams in e_{++} that have an odd number of single continuous paths of h_{QQ} bonds between the root points (a closed loop path involving points 1 and 2, like in the rightmost diagram in (B.8)), is thereby counted as two single paths, one starting at 1 and ending at 2 and vice versa).

Since there are at least two independent paths between the root points in a bridge diagram, the number of cutting h-bonds (the deletion of which would cut all paths between points 1 and 2) in a bridge diagram must be 2 or larger. For a diagram in e_{QQ}, at least one of these cutting h-bonds must be a h_{QQ} bond since each path between 1 and 2 must go through one of the

cutting bonds. If the diagram contains a *cutting pair* of h-bonds, the other bond in this pair must be a h_{NN} bond (since an even number of single h_{QQ} paths between 1 and 2 cannot exist).

Stell [3] has shown how to obtain the large r asymptotic decay of a bridge function consisting of diagrams with h-bonds that have power-law decays. The leading asymptotic term of the bridge function is determined by the diagrams with cutting pairs of h-bonds and the decay is proportional to the product of the h-functions of these bonds. From arguments analogous to those in [3], it follows that $e_{QQ}(r)$ will decay like $h_{QQ}(r)h_{NN}(r)$ provided that $h_{NN}(r)$ and $h_{QQ}(r)$ have power-law decays. (The decay is faster for the diagrams that do not contain a pair of cutting h-bonds.) This result is actually stronger than we need below; it is sufficient that $e_{QQ}(r)$ decays like $h_{QQ}(r)$ or faster (and even this is stronger than what is needed).

For the same reasons as given above when treating the decay of $h_{QQ}(r)h_{NN}(r)$ in equation (B.4), it follows by *reductio ad absurdum* that $e_{QQ}(r)$ cannot contain any power-law term. Thereby, using the arguments stated there, we have demonstrated that $h_{QQ}(r)$ does not decay like a power law when $\gamma_{QQ} = 0$ for a symmetric electrolyte.

Since $e_{NN}(r) = (e_{++}(r) + e_{+-}(r))/2$ for a symmetric electrolyte, it follows from the above analysis that e_{NN} only contains bridge diagrams where all points have an even number of h_{QQ} bonds (including zero). Thus $e_{NN}(r)$ will decay like $h_{NN}^2(r)$, i.e. like r^{-12}.

Before we finish we will for completeness make a comment for the case of symmetric electrolytes with $\gamma_{QQ} \neq 0$. Then, as we have seen, $h_{QQ}(r)$ decays like r^{-10} and it follows from equation (B.4) and the bridge diagram analysis that $c_{QQ}^0(r) - \beta\gamma_{QQ}/r^6$ decays like $h_{QQ}(r)h_{NN}(r)$, i.e. like r^{-16}. In other words, the *second* leading term in the asymptotic expansions of $c_{QQ}^0(r)$ decays like r^{-16}. This term gives a contribution to $h_{QQ}(r)$ that decays like r^{-20}. The second leading term of $h_{QQ}(r)$ originates, however, from the $l = 2$ term in equation (B.2) and decays like r^{-12} in this case. Thus, when the interaction potential makes an r^{-6} contribution to the QQ functions (since $\gamma_{QQ} \neq 0$), a multitude of power-law terms (r^{-10} and higher) appears in $h_{QQ}(r)$.

References

[1] Derjaguin B V and Landau L 1941 *Acta. Phys. Chim. URSS* **14** 633
Verwey E J W and Overbeek J Th G 1948 *Theory of the Stability of Lyophobic Colloids* (Amsterdam: Elsevier)
[2] Enderby J E, Gaskell T and March N H 1965 *Proc. Phys. Soc.* **85** 217
[3] Stell G 1977 *Modern Theoretical Chemistry Series vol 5A Statistical Mechanics: Equilibrium Techniques* ed B J Berne (New York: Plenum) p 47
[4] Aqua J-N and Fisher M E 2004 *J. Phys. A: Math. Gen* **37** L241
[5] Leote de Carvalho R J F, Evans R, Hoyle D C and Henderson J R 1994 *J. Phys.: Condens. Matter* **6** 9275
[6] Brydges D C and Martin Ph A 1999 *J. Stat. Phys.* **96** 1163
[7] Brydges D C and Martin Ph A 2000 *J. Phys. IV France* **10** Pr5–53
[8] Stell G and Lebowitz J L 1968 *J. Chem. Phys* **49** 3706
[9] Mitchell D J M and Ninham B W 1968 *Phys. Rev.* **174** 280
[10] Mitchell D J M and Ninham B W 1978 *Chem. Phys. Lett.* **53** 397
[11] Kjellander R and Mitchell D J M 1994 *J. Chem. Phys.* **101** 603
[12] Stell G 1995 *J. Stat. Phys.* **78** 197
[13] Ulander J and Kjellander R 1998 *J. Chem. Phys.* **109** 9508
[14] Kjellander R and Forsberg B 2004 paper included in B Forsberg 2004 *Fil. Lic. thesis* Göteborg University, Sweden
[15] Morita T and Hiroike K 1960 *Prog. Theor. Phys.* **23** 1003
[16] Hiroike K 1960 *Prog. Theor. Phys.* **24** 317
[17] Allen M P and Tildesley D J 1990 *Computer Simulation of Liquids* (New York: Oxford University Press)
[18] Lebowitz J L and Percus J K 1961 *Phys. Rev.* **122** 1675
[19] Hill T L 1956 *Statistical Mechanics* (New York: McGraw-Hill) appendix 7
[20] Hansen J P and McDonald I R 1986 *Theory of Simple Fluids* (London: Academic) p 374